JOURNAL OF PROPULSION AND POWER
Vol. 22, No. 5, September–October 2006

Characteristics of Dual Transverse Injection in Scramjet Combustor, Part 2: Combustion

Sang-Hyeon Lee*
University of Ulsan, Ulsan, 680-749, Republic of Korea

DOI: 10.2514/1.14185

The combustion characteristics of a dual transverse injection system in a scramjet combustor were studied with numerical methods. The effects of the jet-to-crossflow momentum flux ratio and the distance between injectors on combustion characteristics were investigated. It is shown that the dual injection system has very different combustion characteristics with respect to the single injection system; the burning process of the rear injection flow is strongly influenced not only by the blockage effects but also by the preheating effects due to the chemical reactions of the front injection flow. The dual injection system has a higher burning rate and a higher flame height but more loss of stagnation pressure than the single injection system. It is also shown that there is an optimal distance between injectors for combustion characteristics and that the optimal distance increases as the jet-to-crossflow momentum flux ratio increases.

Nomenclature

J = jet-to-crossflow momentum flux ratio
r_{OH} = effective radius of OH radical
W = molecular weight
η_b = burning efficiency
σ_{OH} = standard deviation of OH radical distribution

Subscript

r = chemical reaction step

Introduction

THE present study follows part 1 of the present paper [1] that presented the mixing characteristics of a dual transverse injection system in a scramjet combustor. In the present study, the combustion characteristics of a dual transverse injection system are presented. The physical phenomena, including burning process in a dual transverse injection system, are even more complex. Figure 1 shows the schematic view of the burning processes such as ignition and flame propagations. The bow shock wave in front of the transverse jet raises the air temperature so high that the mixture of air and hydrogen in the region right after the shock wave is self-ignited. There is no self-ignition in the separation region because the mixture temperature is not high enough. After the ignition, the flame propagates through the mixture flow encountering vortex pairs, separation bubbles, horseshoe vortices, wake flows, etc. Thus, the flame surfaces are formed surrounding the jet boundaries.

There have been many research activities to investigate supersonic combustion in the scramjet combustors [2–11]. It is known that the combustion process in a scramjet combustor is strongly influenced and limited by the fuel–air mixing process [2–5]. Lee et al. [5] studied the parallel injection system of a scramjet combustor and reported that the combustion characteristics are determined exclusively by the mixing process. This could be true in a parallel injection case because the flows are supersonic in most regions and thus the flow time scales are much shorter than mixing time scales. However, as mentioned by Segal et al. [4] and Mitani et al. [8], the combustion in a supersonic combustor would be controlled by either the mixing rate or the chemical reaction rate according to the gradients of thermo-fluid-dynamic variables and the Mach number distributions in the flow fields. Also, in a dual transverse injection system, there are many subsonic regions such as recirculation zones and the regions between injectors in which the mixing time scale is on the order of the flow time scale. In the far fields the burning process would be controlled by the diffusion process, but in the near fields the ignition and burning process between two injectors would change the flow fields and thermodynamic situation. Thus, the burning process would have influences on the flow fields and the mixing process. Therefore, it is necessary to investigate the combustion characteristics of a dual transverse injection system. Another important problem is the autoignition in a scramjet combustor. Recent research [12–14] reported the importance of inlet air temperature for autoignition in the supersonic combustors. Li et al. [13] suggested that the minimum temperature for autoignition for a hydrogen–air mixture is about 1100 K. The flow and thermodynamic conditions were determined to satisfy the requirement. However, it is well known that autoignition is also influenced by the other conditions such as flow structure and combustor geometry. Thus, it is necessary to check the possibility of autoignition for the flow and thermodynamic condition of the present study.

The main objective of the present study is to analyze the combustion characteristics of a dual injection system in a scramjet combustor and to search for the relationships between mixing characteristics and combustion characteristics. One of the key questions of the present study is whether or not the combustion characteristics are determined exclusively by mixing characteristics. As mentioned in part 1 of this paper [1], the blockage effects due to the flow blocking by the front injection flow have significant influence on the mixing process of the rear injection flow and thus the global mixing characteristics. Thus, the blockage effects would have significant influence on combustion characteristics. However, conversely, the burning process at near fields of the injection system would have significant influence on the mixing process by changing the thermodynamics and flow fields. The heat addition due to the burning of the front injection flow might lead to a remarkable change of flow fields between injectors and thus lead to a change of blockage effects with respect to the nonreacting case. The increase of temperature due to chemical reactions would reduce the Mach number and thus reduce the strength of the shock waves ahead of the rear injector. Even in the far field the diffusion coefficients would increase due to the increase of temperature. Therefore, a detailed investigation is necessary. Another concern is if the concept of the optimal distance between injectors for mixing characteristics is maintained for combustion characteristics, and whether or not the

Received 25 October 2004; revision received 12 January 2006; accepted for publication 21 January 2006.

*Associate Professor, Department of Aerospace Engineering; email: lsh@mail.ulsan.ac.kr

optimal distance between injectors for combustion characteristics coincided with that for mixing characteristics. Because the air inflow is supersonic and most regions except near fields of the injection system are supersonic, the rear injection flow would have less influence on the front injection flow, which means that the blockage effects still have the dominant role on the mixing process. Thus, the optimal distance between injectors for combustion characteristics would still exist. However, it is not clear whether the optimal distance for combustion characteristics is longer than that for mixing characteristics. In the present study, three-dimensional Navier–Stokes equations with a reliable chemical reaction model for the hydrogen–air mixture were calculated to search for answers to these questions.

The main parameters for combustion characteristics considered in the present study are burning rate or burning efficiency, flame height, and stagnation pressure loss. Burning rate is the most important parameter of combustion characteristics, because faster burning ensures higher thrust and a shorter combustor length. Flame height is also an important parameter, because the flame should be far enough away from the combustor wall to enhance fuel burning and to avoid wall heating in a scramjet combustor. An excessive loss of stagnation pressure should be avoided, because the loss of stagnation pressure results in a loss of thrust.

Calculation Methods

Three-dimensional Navier–Stokes equations with a chemical kinetics model are solved to simulate the burning process of the dual transverse injection system. The governing equations are expressed in vector form as follows:

$$\frac{\partial Q}{\partial t} + \frac{\partial E_j}{\partial x_j} = \frac{\partial E_{vj}}{\partial x_j} + S_T + S_C \tag{1a}$$

$$Q = \begin{bmatrix} \rho_s \\ \rho u_i \\ \rho e_o \\ \rho k \\ \rho \omega \end{bmatrix}, \qquad E_j = \begin{bmatrix} \rho_s u_j \\ \rho u_i u_j + \delta_{ij} \\ \rho h_o u_j \\ \rho k u_j \\ \rho \omega u_j \end{bmatrix},$$

$$E_{vj} = \begin{bmatrix} \rho_s u_{sj}^d \\ \tau_{ij} \\ \tau_{jk} u_k - q_j \\ (\mu_L + \sigma^* \mu_T) \frac{\partial k}{\partial x_j} \\ (\mu_L + \sigma \mu_T) \frac{\partial \omega}{\partial x_j} \end{bmatrix}, \qquad S_T = \begin{bmatrix} 0 \\ 0 \\ 0 \\ P_k \\ P_\omega \end{bmatrix} \quad \text{and} \tag{1b}$$

$$S_C = \begin{bmatrix} \dot{\rho}_s \\ 0 \\ 0 \\ 0 \\ 0 \end{bmatrix}$$

The details of the Navier–Stokes equations and the turbulence model can be found in part 1 of the present paper [1]. The term S_C is the chemical kinetic source vector. Nine chemical species (H, O, OH, H_2O, HO_2, H_2O_2, H_2, O_2, and N_2) are considered. These chemical species are treated as ideal gases. The chemical kinetic source terms are represented as follows:

$$\dot{\rho}_s = W_s \sum_r (\nu_{sr}^b - \nu_{sr}^f)(q_r^f - q_r^b) \tag{2a}$$

$$q_r^f = k_r^f \prod_s \left(\frac{\rho_s}{W_s}\right)^{\nu_{sr}^f} \quad \text{and} \quad q_r^b = k_r^b \prod_s \left(\frac{\rho_s}{W_s}\right)^{\nu_{sr}^b} \tag{2b}$$

where the symbols ν_{sr}^f and ν_{sr}^b are the forward and backward reaction coefficients of the species s in the rth reaction step, respectively. The symbols k_r^f and k_r^b are the forward and backward rate constants in the rth reaction step, respectively. The Jachimowski's hydrogen–air chemical kinetic model [15] developed for calculating the supersonic combustion in a scramjet is used to calculate the chemical kinetic source terms. The reaction steps including nitrogen are ignored for convenience.

Most of the numerical methods for calculating flow fields are the same as in part 1 of the present paper [1]. The chemical kinetic source term is so stiff that the Jacobian of the chemical kinetic source term should be included in the calculations. Thus, the time-integration algorithm was the lower-upper symmetric successive overrelaxation scheme [16] instead of the lower-upper symmetric Gauss–Seidel scheme.

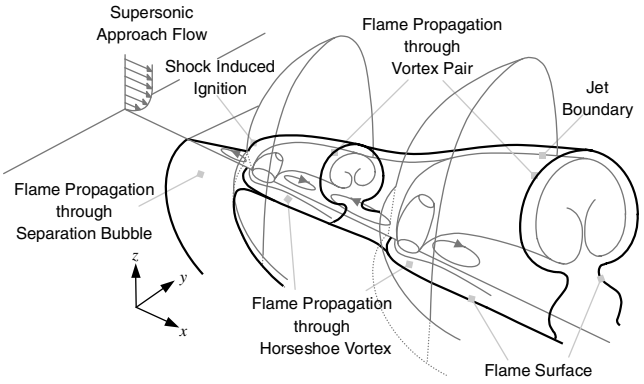

Fig. 1 Schematic view of ignition and flame propagations of the dual transverse injection system.

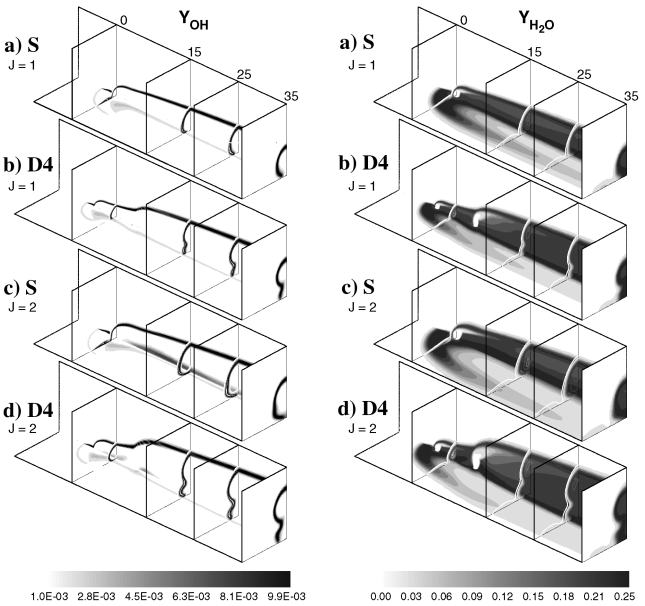

Fig. 2 Comparison of combustion process between single injection systems and dual injection systems.

Results

Overall Combustion Characteristics

To compare the overall trends of the combustion characteristics between the dual injection system and the single injection system, the distributions of mass fraction of the OH radical and water vapor are plotted in Fig. 2. Figures 2a and 2b compare the burning processes between model S and model D4 when the magnitude of the jet-to-crossflow momentum flux ratio J is 1.0, whereas Figs. 2c and 2d compare the burning processes between model S and model D4 when the value of J is 2.0. In Fig. 2, the left column shows the distribution of the mass fraction of OH radical, whereas the right column shows the distribution of the mass fraction of water vapor (H_2O). The inlet

air temperature of the present study is slightly lower than that suggested by Li et al. [13], but there are autoignitions at the regions immediately after the strong bow shock waves. After that the flames propagated through the flows such as vortex pair flow, recirculation flow, and separation flow. The OH radical is mainly distributed on the contact surface between the jet flow and the airflow, which implies that the flame is located on the contact surface between the airflow and hydrogen jet flow and thus is a diffusion flame. The water vapor is mainly distributed on the flame surface and within the flame surface but is scarcely distributed outside of the flame surface, which is due to the fact that the mass diffusion between water vapor and hydrogen is higher than between water vapor and air.

The case with a higher magnitude of J has a higher flame position and a larger flame surface in a y–z plane in each model, which is consistent with the fact that the case with a higher magnitude of J in the nonreacting flow has a higher penetration and a larger mixing surface. Model D4 has a higher flame position and larger flame surface in a y–z plane than model S when the values of J are the same, which is consistent with the fact that the dual injection system has a higher penetration and a larger mixing surface in nonreacting flows than the single injection system. Thus, it can be stated that a dual injection system has better combustion characteristics than the single injection system and that the combustion characteristics are mainly determined by the mixing characteristics.

As mentioned during the analysis of the mixing characteristics in part 1 of the present paper [1], the augmentation of the mixing characteristics is largely due to the "blockage effect" in which the front injection flow blocks airflow and reduces the momentum of the airflow towards the rear injection flow. Therefore, the effective jet-to-crossflow momentum flux ratio of the rear injection flow may increase, which might assist the rear injection flow in expanding more strongly, to collide with airflow and thus to have stronger chemical reactions. At this point, another question about the blockage effects could be asked: Is the strength of the blockage effects the same as those estimated with the nonreacting calculations? To investigate the blockage effects in detail, the fields of pressure, temperature, and Mach number near injection holes in the x–z plane are plotted in Fig. 3. Darker regions in Fig. 3 have higher values of pressure, temperature and Mach number, respectively. The highest values of pressure, temperature, and Mach number are $6.7p_\infty$, 2617 K, and 5.3, respectively. The figures in the left column show the fields of nonreacting flows, whereas the figures in the right column show the fields of reacting flows. The reacting case has a stronger bow shock wave and a stronger separation shock wave in front of the front injection flows than the nonreacting case because of the strong generation of heat energy in the reacting case. The reacting case has a higher pressure in the region right after the front injector, which is due to the stronger shock waves. However, the reacting case has weaker pressure in the region ahead of the rear injection flow. These phenomena can be explained with the comparison of Mach number distributions ahead of the rear injection flow. The Mach numbers in the regions ahead of the rear injection flow in the reacting cases are lower than in the nonreacting cases. The reduction of Mach numbers results from the temperature increases in the regions ahead of the rear injection flow due to the burning of the front injection flow, which can be called "preheating effects." The reduction of Mach numbers in the regions ahead of the rear injection flow results in a reduction of the strength of the shock waves and thus results in a reduction of static pressure. It also should be noted that model D7 shows a drastic decrease of the pressure in the region ahead of the rear injection flow in the reacting case with respect to that in the nonreacting case. Also, model D3 shows a little decrease of pressure in the region ahead of the rear injection flow in the reacting case with respect to that in the nonreacting case. Thus, it can be stated that the preheating effects increased as the distance between injectors increased, which suggested that the optimal distance between injectors for combustion characteristics would be longer than is expected with the nonreacting calculations.

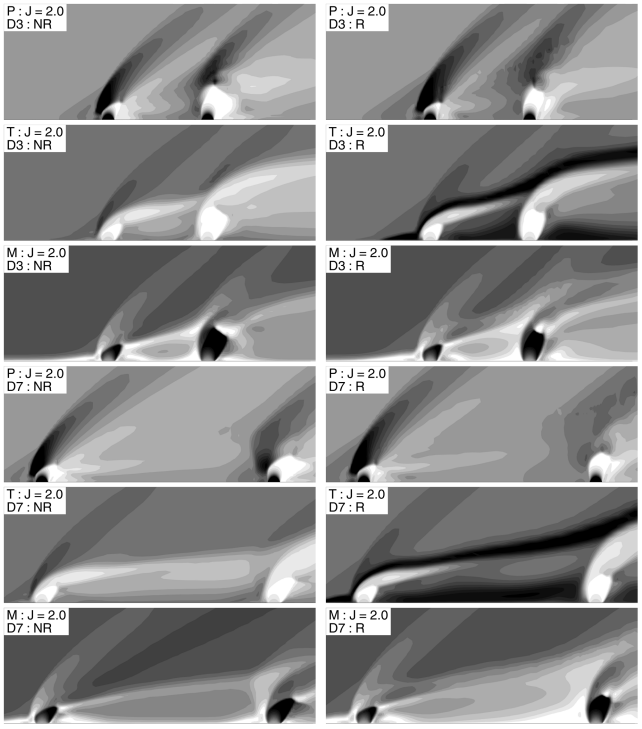

Fig. 3 Comparison of pressure field P, temperature field T, and Mach number field M between the nonreacting case (NR, left column) and the reacting case (R, right column).

The variations of the height of the Mach disk due to the distance between injectors and due to the magnitude of J are plotted to confirm the changes of blockage effects mentioned in the preceding paragraph. Figure 4 shows the variations of the height of the Mach disks due to the magnitude of J and due to the distance between injectors. The case with a higher magnitude of J shows a higher height of the Mach disk and a larger difference of the height of the Mach disk between the front and rear injection flows. The Mach disk height of the front injection flow in the dual injection system is smaller than that of the single injection system because the diameter of the injection hole of the dual injection system is smaller than that of the single injection system. The heights of the Mach disks of the rear injection flows are higher than those of the front injection flows due to the blockage effects. These trends are the same as those of the nonreacting cases. The heights of the Mach disks of the reacting cases in models S, D1, and D2 are almost the same as those of the nonreacting cases. However, there are drastic changes in the heights of the Mach disks of the rear injection flows, with respect to those of nonreacting cases, in the models with longer distance between injectors: in models D3, D4, D5, and D7 when the magnitude of J is

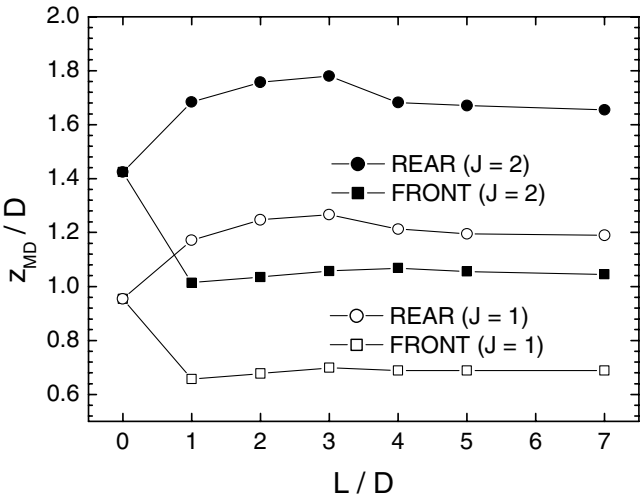

Fig. 4 Variations of height of Mach disk due to distance between injectors.

1.0 and in models D5 and D7 when the magnitude of J is 2.0. As shown in part 1 of the present paper [1] regarding the mixing characteristics, the height of the Mach disk of the rear injection flow decreased steeply in the nonreacting cases. However, the height of the Mach disk of the rear injection flow in the reacting case is nearly maintained with the increase of the distance between injectors. This implies that the blockage effects are strengthened due to the preheating effects and that the preheating effects grow with the increase of the distance between injectors. This is consistent with the changes of the pressure fields ahead of the rear injection flows due to the preheating effects. Thus, the optimal distance between injectors would be longer than is expected with the analysis of mixing characteristics of nonreacting cases.

Streamwise Vorticities

It is well known that streamwise vorticity has a great influence on the mixing process and thus on the burning process in high-speed flows [17,18]. To represent the effects of streamwise vorticity as a scalar in a y–z plane, the circulation is plotted. The histories of circulation of all models are plotted in Fig. 5. There are two jumps of circulation at the front and rear injection holes in the dual injection systems, whereas there is a single jump of circulation in the single injection system. The first peak of the circulation in the dual injection system is smaller than the peak of the single injection system because the diameter of the injection hole of the dual injection system is smaller than that of the single injection system. The circulation of a dual injection system is higher than of the single injection system. The strengths of the first jumps are the same, whereas the strengths of the second jumps depend on the distance between injectors. The strength of circulation is closely related to the magnitude of J. In the case of a higher magnitude of J there is stronger streamwise vorticity than with a lower magnitude of J. Also, strength of circulation is closely related to the distance between injectors. The strengths of the second jumps increased as the distance between injectors increased until a critical distance was reached but then decreased after that critical distance. These facts are the same as those of the nonreacting cases. However, there are some changes of the features of the circulations due to the chemical reactions. The circulation of the reacting case is about 20% higher than of nonreacting cases. These increases of circulation are due to the stronger shock waves formed ahead of the front injection flow in the reacting case with respect to those in the nonreacting case, as mentioned in the previous section.

Burning Rates

The burning rate is one of the most important parameters of combustion characteristics. Even though there are many definitions of burning rate, in the present study two kinds of burning rate are introduced: production rate of water vapor and consumption rate of hydrogen fuel. Figure 6a shows the variations in the production of water vapor due to the distance between injectors and the magnitude of J, whereas Fig. 6b shows the variations in the consumption of hydrogen fuel due to the magnitude of J and due to the distance between injectors. (Δm_{H_2} is the difference of mass flow rate between the nonreacting case and the reacting case.) The trend of the production rate of water vapor is almost the same as that of the consumption rate of hydrogen fuel, which is due to the fast chemical kinetics of the hydrogen–air reaction mechanism as expected. Thus, the production rate of water vapor will hereafter be considered as the burning rate, for convenience. The production of water vapor is strongly related to the magnitude of J. The case with a higher magnitude of J has a higher production rate of water vapor and a

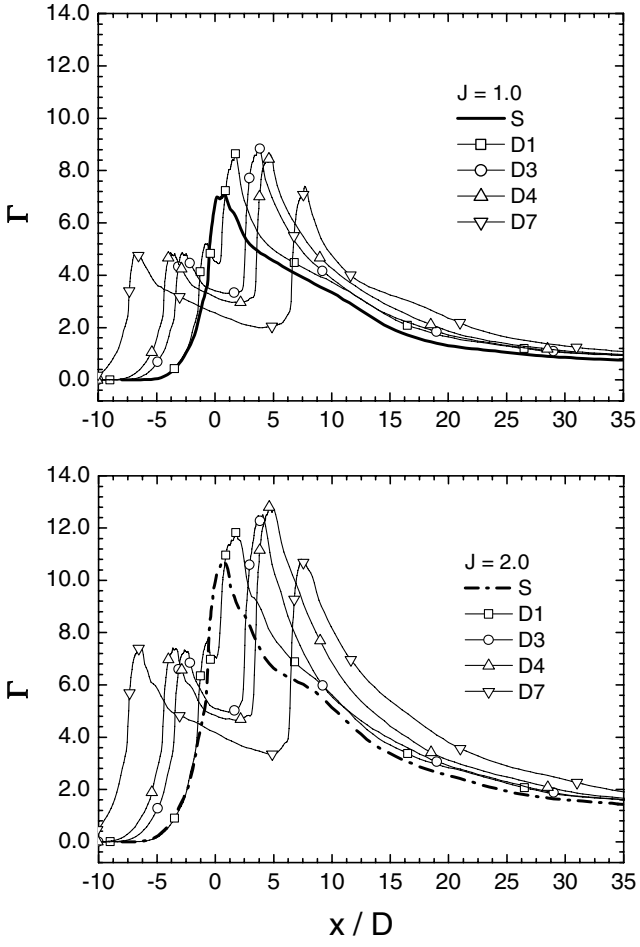

Fig. 5 Comparison of circulation normalized by diameter of the injection hole and velocity of inflow air.

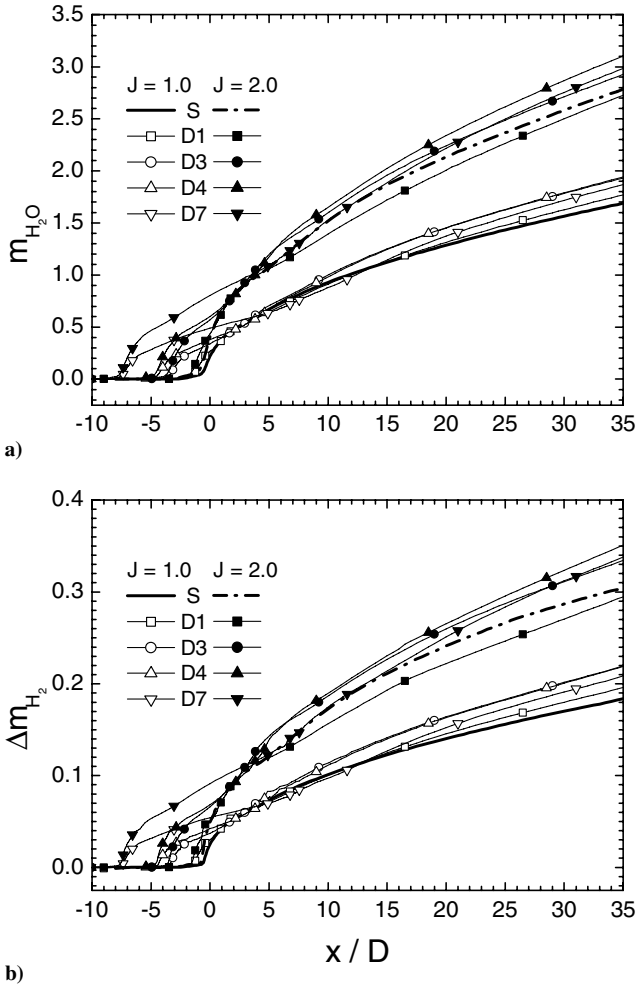

Fig. 6 Comparison of burning rate: a) mass flow rates of water vapor and b) consumption rates of hydrogen fuel.

higher slope of production rate. This can be explained with the facts that the case with a higher magnitude of J has a higher mass flow rate, a higher penetration, and a larger effective radius of hydrogen fuel as mentioned during the analysis of mixing characteristics. Also, the production rate of water vapor is closely related to the distance between injectors. Models D3 and D4 have almost the same production rates of water vapor and also have higher production rates than the other models when the magnitude of J is 1.0 although Model D4 has a higher production rates than any other model when the magnitude of J is 2.0. This implies that there is an optimal distance between injectors for combustion characteristics and that the optimal distance between injectors increases as the magnitude of J increases, which is consistent with the analysis of mixing characteristics. However, it should be noted that model D7 has a higher slope of production rate and finally has a higher production rate at the far downstream especially when the magnitude of J is 2.0, which is not consistent with the expectation based on the analysis of mixing characteristics. This is due to the preheating effects as mentioned in the preceding sections. The case with a higher magnitude of J has stronger preheating effects due to higher heat addition and a wider preheating cross-section area.

The concept of the burnt fraction or burning efficiency is adopted to quantify the burning capabilities. Burning efficiency is evaluated by the consumed fraction of hydrogen mass flow with respect to the hydrogen mass flow in the nonreacting case as follows:

$$\eta_b(x) = 1 - \frac{\oint\int \rho_{H_2} u \,\mathrm{d}y\,\mathrm{d}z|_{\text{reacting}}}{\oint\int \rho_{H_2} u \,\mathrm{d}y\,\mathrm{d}z|_{\text{nonreacting}}} \tag{3}$$

Figure 7 shows the variations of the burning efficiencies due to the magnitude of J and due to the distance between injectors. In Fig. 7 burning efficiency is evaluated by the ratio of consumed hydrogen mass flow with respect to the hydrogen mass flow in the nonreacting case. Burning efficiencies are closely related to the magnitude of J. The case with a higher magnitude of J shows lower burning efficiencies than that with a lower magnitude of J, which is consistent with the fact that the case with a higher magnitude of J has a lower mixing efficiency as mentioned in part 1 of the present paper [1]. The burning efficiency of a dual injection system depended on the distance between injectors. Models D3 and D4 show almost the same burning efficiency and have a higher burning efficiency than the other models when the magnitude of J is 1.0, whereas models D4 and D5 have almost the same burning efficiency and have a higher burning efficiency when the magnitude of J is 2.0. These trends are almost the same as those mentioned in the analysis of the mixing characteristics. However, the variation of burning efficiency did not coincide exactly with the variation of mixing efficiency estimated with the nonreacting calculations. Model D2 has a higher mixing efficiency than model D4 when the magnitude of J is 1.0, whereas model D4 has a higher burning efficiency than model D2. Also, model D3 has almost the same mixing efficiency as model D4 when the magnitude of J is 2.0, whereas model D5 has a higher burning efficiency than model D3. These facts suggest that the optimal distance for burning efficiency is longer than expected with nonreacting calculations, which is due to the preheating effects as mentioned in the preceding sections.

The effective radius of the OH radical and the standard deviation of the effective radius are introduced to estimate the relationship between burning rates and flame structures. The case with a larger effective radius would have a wider distribution of the OH radical or a larger flame, whereas the case with a larger standard deviation would have a more complex flame structure or a wider flame surface:

$$r_{OH}(x) = \frac{\oint\int \rho_{OH}|\boldsymbol{r} - \boldsymbol{c}|\,\mathrm{d}y\,\mathrm{d}z}{\oint\int \rho_{OH}\,\mathrm{d}y\,\mathrm{d}z} \tag{4a}$$

$$\sigma^2_{OH}(x) = \frac{\oint\int \rho_{OH}(|\boldsymbol{r} - \boldsymbol{c}| - r_{OH})^2\,\mathrm{d}y\,\mathrm{d}z}{\oint\int \rho_{OH}\,\mathrm{d}y\,\mathrm{d}z} \tag{4b}$$

The vectors $\boldsymbol{r}$ and $\boldsymbol{c}$ are the position vector at a location in a y–z plane and the position vector of the mass center of the OH radical, respectively. Figure 8 shows the comparison of the effective radii of the OH radical in a y–z plane. The first peak of the effective radius in the dual injection system is smaller than the peak of the single injection system because the diameter of the injection hole in the dual injection system is smaller than that of the single injection system. The effective radius is related to the magnitude of J, but the degree of variation is relatively small considering that the case with twice the magnitude of J has twice the mass flow rate. The case in which the

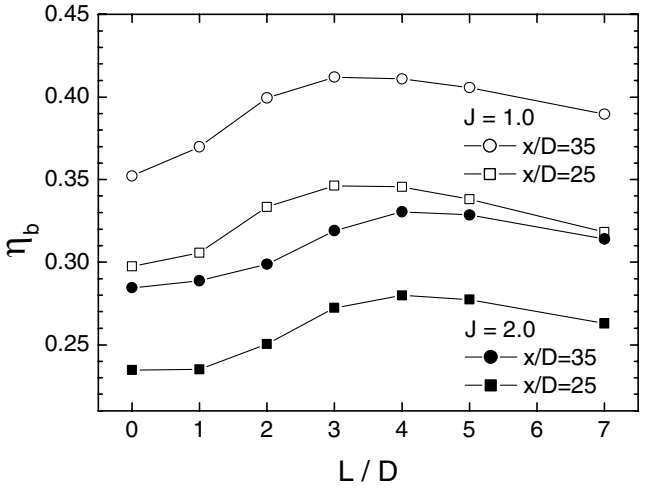

Fig. 7 Comparison of burning efficiencies at $x/D = 25$ and 35.

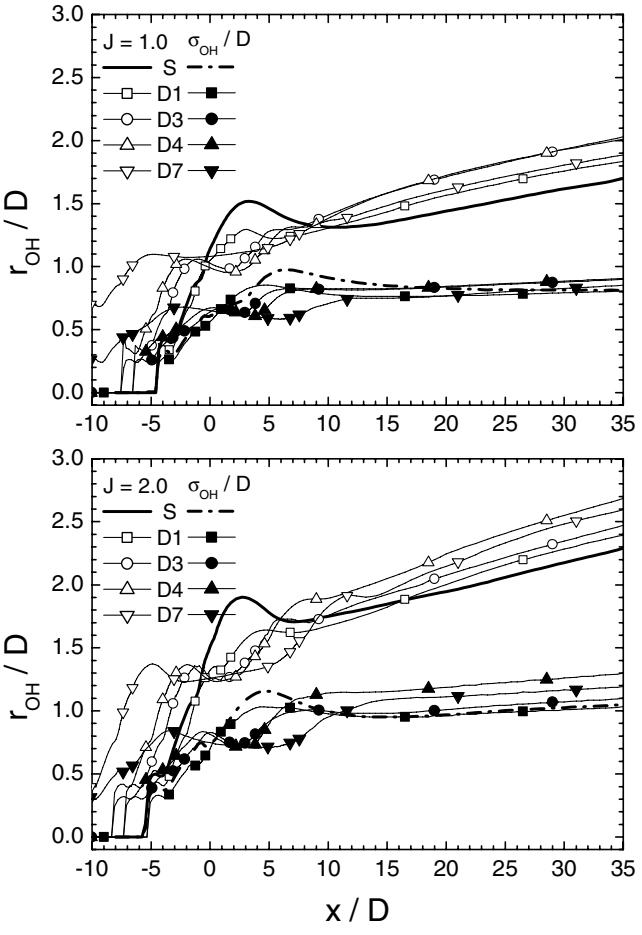

Fig. 8 Comparison of effective radii of OH radical r_{OH} and standard deviations of effective radius of OH radical σ_{OH}.

magnitude of J is 2.0 has a slightly larger effective radius and a slightly larger standard deviation than the case in which the magnitude of J is 1.0. This means that the relative flame surface decreased as the magnitude of J increased, which is consistent with the analysis of burning rate mentioned in the preceding paragraph. The effective radius is strongly related to the distance between injectors. Models D3 and D4 show almost the same radii and standard deviations and have larger effective radii of the OH radical and standard deviations than the other models when the magnitude of J is 1.0, whereas model D4 has the largest effective radius of the OH radical and the largest standard deviation when the magnitude of J is 2.0. These facts are consistent with the facts that models D3 and D4 have higher burning rates than the other models when the magnitude of J is 1.0, whereas model D4 has the highest burning rate when the magnitude of J is 2.0, as mentioned during the analysis of burning rates. Thus, it can be stated that the concepts of the effective radius and its standard deviation are good indicators of burning capabilities. In the nonreacting calculations, model D3 has a larger effective radius of hydrogen and its standard deviation case than model D7. However, in the nonreacting calculations, model D3 has a smaller effective radius of the OH radical and its standard deviation than model D7. This reversal is due to the preheating effects as mentioned in the preceding sections.

Flame Heights

In a real scramjet combustor, the flame region should be separated as far from the combustor walls as possible to minimize wall heating and to maximize combustion efficiency. Thus, the variations of flame height due to the magnitude of J and due to the distance between injectors are investigated. The flame height is estimated by the mass center of the OH radical from the lower wall as follows:

$$Z_{\mathrm{OH}}(x) = \frac{\oint \int \rho_{\mathrm{OH}} z \, \mathrm{d}y \, \mathrm{d}z}{\oint \int \rho_{\mathrm{OH}} \, \mathrm{d}y \, \mathrm{d}z} \tag{5}$$

Figure 9 shows the comparison of flame height. The reference location $z = 0$ is the lower wall. In every case, the flame height increased rapidly right after the injection, but the increasing rate of flame height decreased gradually and finally became nearly constant at the far field. The flame height of a dual injection system has a higher penetration than of the single injection system. The flame heights are closely related to the magnitude of J. The case with a higher magnitude of J has a higher flame height. This is due to the fact that the jet flow with a higher magnitude of J has a stronger inertia and penetrates higher into the crossflow than the flow with a lower magnitude of J, which is matched well with the analysis of the penetration distance estimated with the nonreacting calculations. There is also a strong relationship between flame height and the distance between injectors. Models D3 and D4 show nearly the same flame height and have higher flame heights than the other models when the magnitude of J is 1.0, whereas model D4 has the highest flame height when the magnitude of J is 2.0. These facts suggest that there is an optimal distance between injectors for flame height and that the optimal distance increases as the magnitude of J increases.

Stagnation Pressure Losses

Generally, the mixing and burning process produces losses of stagnation pressure that result in a loss of thrust. Therefore, it should be determined whether or not there are additional losses of stagnation pressure due to mixing and combustion augmentations. Figure 10 shows the histories of average stagnation pressure along the streamwise direction normalized by the stagnation pressure of air inflow. All models show very similar histories of stagnation pressures; the stagnation pressure decreases slowly in the region before the front injection holes but begins to decrease very steeply from the region right after the injection holes. These rapid decreases of stagnation pressure are due to the bow shock wave and the separation shock wave formed in front of the jet flows and due to the mixing and burning of hydrogen fuel. It should be noted that the reacting case suffers more loss in stagnation pressure than a nonreacting case by 2 or 3% (see the analysis of nonreacting calculations), which is due to the heat addition and thus due to the increase of entropy in the reacting case.

Stagnation pressure losses are strongly related to the magnitude of J. The case of a higher magnitude of J shows more loss of stagnation pressure. The increase of stagnation pressure loss with the increase in the magnitude of J is due to the stronger shock waves and stronger streamwise vorticity. In general, a dual injection system shows more loss of stagnation pressure than the single injection system, which is due to the augmentations of mixing rate, penetration, and burning rate. However, the increase of stagnation pressure loss in dual injection systems is not too detrimental because the combustion is improved when compared with that of the single injection system. Model D1 shows less loss of stagnation pressure than the single injection system and is an exceptional case. This can be explained with the analysis of burning rate mentioned in the preceding section where model D1 shows a less or slightly higher burning rate and penetration than the single injection system and with the fact that the strength of the shocks in front of the injection flows is much weaker than the single injection system.

Conclusion

In the present study, the combustion characteristics of the dual injection system in a scramjet combustor are studied with numerical methods. Two kinds of parametric studies are conducted to

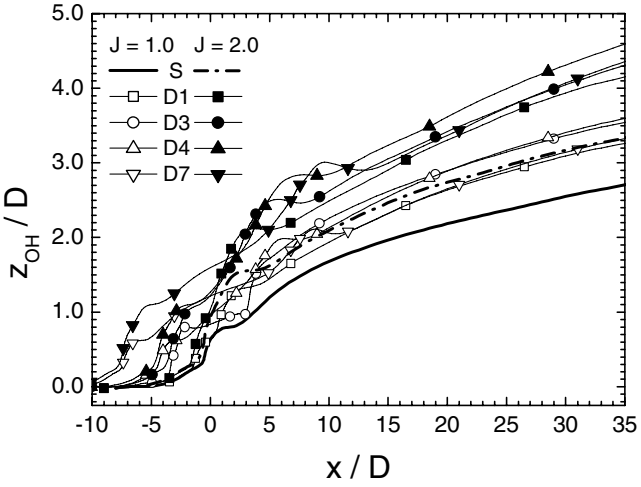

Fig. 9 Comparison of flame height expressed by the averaged height of OH radicals.

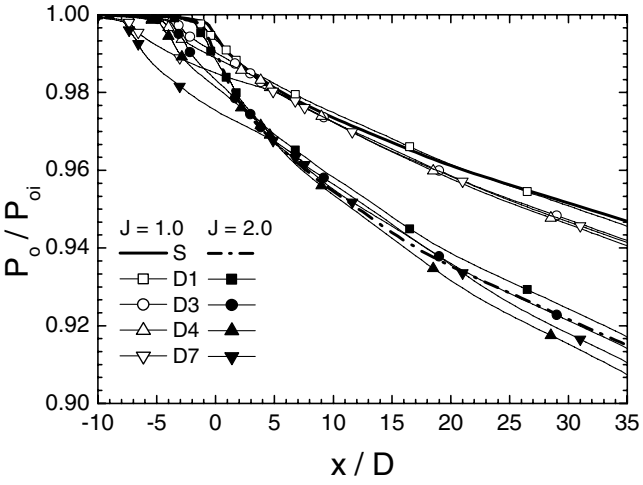

Fig. 10 Comparison of stagnation pressure normalized by the stagnation pressure of inflow.

investigate the variations of combustion characteristics due to the jet-to-crossflow momentum flux ratio, J and due to the distance between injectors.

The combustion characteristics of a dual injection system are very different from those of the single injection system. A combustor with a dual injection system has better combustion characteristics than the single injection system: higher burning rates and higher flame heights. The rear injection flow in a dual injection system is strongly influenced by the front injection flow. The rear injection flow has a higher flow expansion due to the blockage effects, which is expected with nonreacting calculations. However, the blockage effects in reacting cases are stronger than is expected with the nonreacting calculations, which is due to the preheating effects. The preheating effects led to the augmentation of flow expansion and the improvements of the ignition and burning of the rear injection flow. The case with a longer distance between injectors has higher preheating effects due to more burning of the front injection flows. Thus, the effects of chemical reactions should be considered to investigate the performance of a dual transverse injection system in a scramjet combustor.

The combustion characteristics of the dual transverse injection systems are strongly related to the jet-to-crossflow momentum flux ratio J. The case with a higher magnitude of J has a lower burning rate and a lower burning efficiency but a higher flame height. The combustion characteristics in a dual injection system are closely related to the distance between injectors. The burning rate and flame height increased as the distance between injectors increased until a critical distance was reached and decreased after that critical distance. Thus, there existed an optimal distance between injectors for combustion characteristics, and the optimal distance between injectors for combustion characteristics increased as the magnitude of J increased. However, the optimal distance for combustion characteristics is longer than is expected with the optimal distance between injectors for mixing characteristics, which is due to the preheating effects.

Stagnation pressure loss is strongly related to the magnitude of J. The case with a higher magnitude of J shows more loss of stagnation pressure. A dual injection system suffered more loss of stagnation pressure with respect to the single injection system. The case with a higher burning rate and a higher flame height suffered more loss of stagnation pressure. However, the increased loss of stagnation pressure of a dual injection system is not so great considering the enhancement of combustion characteristics with respect to that of the single injection system.

Acknowledgment

This study is supported by the Research Program of University of Ulsan.

References

[1] Lee, S-H., "Characteristics of Dual Transverse Injection in Scramjet Combustor Part 1: Mixing," *Journal of Propulsion and Power*, Vol. 22, No. 5, 2006, pp. 1012–1019.

[2] Abbitt, J. D., III, Segal, C., McDaniel, J. C., Krauss, R. H., and Whitehurst, R. B., "Experimental Supersonic Hydrogen Combustion Employing Staged Injection Behind a Rearward-Facing Step," *Journal of Propulsion and Power*, Vol. 9, No. 3, 1993, pp. 472–478.

[3] Billig, F. S., "Research on Supersonic Combustion," *Journal of Propulsion and Power*, Vol. 9, No. 4, 1993, pp. 499–514.

[4] Segal, C., Krauss, R. H., Whitehurst, R. B., and McDaniel, J. C., "Mixing and Chemical Kinetics Interactions in a Mach 2 Reacting Flow," *Journal of Propulsion and Power*, Vol. 11, No. 2, 1995, pp. 308–314.

[5] Lee, S-H., Jeung, I-S., and Yoon Y., "Computational Investigation of Shock-Enhanced Mixing and Combustion," *AIAA Journal*, Vol. 35, No. 12, 1997, pp. 1813–1820.

[6] O'Byrne, S., Doolan, M., Olsen, S. R., and Houwing A. F. P., "Measurement and Imaging of Supersonic Combustion in a Model Scramjet Engine," *Shock Waves*, Vol. 9, No. 4, 1999, pp. 221–226.

[7] Tomioka, S., Murakami, K., Kudo, K., and Mitani, T., "Combustion Test of a Staged Supersonic Combustor with a Strut," *Journal of Propulsion and Power*, Vol. 17, No. 2, 2001, pp. 293–300.

[8] Mitani, T., Chinzei, N., and Kanda, T., "Reaction and Mixing Controlled Combustion in Scramjet Engine," *Journal of Propulsion and Power*, Vol. 17, No. 2, 2001, pp. 308–314.

[9] Mathur, T., and Billig, F. S., "Supersonic Combustor Experiment with a Cavity Based Injector," *Journal of Propulsion and Power*, Vol. 17, No. 6, 2001, pp. 1305–1312.

[10] Goyne, C. P., McDaniel, J. C., Quagliaroli, T. M., Krauss, R. H., and Day S. W., "Dual-Mode Combustion of Hydrogen in a Mach 5 Continuous-Flow Facility," *Journal of Propulsion and Power*, Vol. 17, No. 6, 2001, pp. 1313–1318.

[11] Baurle, R. A., and Eklund, D. R., "Analysis of Dual-Mode Hydrocarbon Scramjet Operation at Mach 4–6.5," *Journal of Propulsion and Power*, Vol. 18, No. 5, 2002, pp. 990–1002.

[12] Riva, G., Daminelli, G., and Reggiori, A., "Hydrogen Autoignition and Combustion in Supersonic Flow at Low Equivalence Ratio," *Journal of Propulsion and Power*, Vol. 13, No. 4, 1997, pp. 532–537.

[13] Li, J., Yu, G., Zhang, Y., Li, Y., and Qian, D., "Experimental Studies on Self-Ignition on Hydrogen/Air Supersonic Combustion," *Journal of Propulsion and Power*, Vol. 13, No. 4, 1997, pp. 538–542.

[14] Kanda, T., Chinzei, N., Kudo, K., Murakami, A., and Hiraiwa, T., "Autoignited Combustion Testing in a Water-Cooled Scramjet Combustor," *Journal of Propulsion and Power*, Vol. 20, No. 4, 2004, pp. 657–664.

[15] Jachimowski, C. J., "An Analytical Study of the Hydrogen-Air Reaction Mechanism with Application to Scramjet Combustion," NASA TR-2791, 1988.

[16] Shuen, J. S., and Yoon, S., "Numerical Study of Chemically Reacting Flows Using a Lower-Upper Symmetric Successive Overrelaxation Scheme," *AIAA Journal*, Vol. 27, No. 12, 1989, pp. 1752–1760.

[17] Lee, S-H., Jeung, I-S., and Yoon, Y., "Computational Investigation of Shock-Enhanced Mixing: Application to Cicular Cross-Section Combustor," *AIAA Journal*, Vol. 36, No. 11, 1998, pp. 2055–2062.

[18] Waitz, I. A., Marble, F. E., and Zukoski, E. E., "Investigation of a Contoured Wall Injector for Hypervelocity Mixing Augmentation," *AIAA Journal*, Vol. 31, No. 6, 1993, pp. 1014–1021.

J. Oefelein
Associate Editor